Follow us @BoneJointRes

Freely available online OPEN ACCESS

BJR

BONE FRACTURE

# Osteocyte-specific dentin matrix protein 1

## THE ROLE OF MINERALIZATION REGULATION IN LOW-MAGNITUDE HIGH-FREQUENCY VIBRATION ENHANCED OSTEOPOROTIC FRACTURE HEALING

**M. C. M. Li,**
**S. K-H. Chow,**
**R. M. Y. Wong,**
**B. Chen,**
**J. C. Y. Cheng,**
**L. Qin,**
**W-H. Cheung**

*From The Chinese University of Hong Kong, Hong Kong, China*

### Aims

There is an increasing concern of osteoporotic fractures in the ageing population. Low-magnitude high-frequency vibration (LMHFV) was shown to significantly enhance osteoporotic fracture healing through alteration of osteocyte lacuno-canalicular network (LCN). Dentin matrix protein 1 (DMP1) in osteocytes is known to be responsible for maintaining the LCN and mineralization. This study aimed to investigate the role of osteocyte-specific DMP1 during osteoporotic fracture healing augmented by LMHFV.

### Methods

A metaphyseal fracture was created in the distal femur of ovariectomy-induced osteoporotic Sprague Dawley rats. Rats were randomized to five different groups: 1) DMP1 knockdown (KD), 2) DMP1 KD + vibration (VT), 3) Scramble + VT, 4) VT, and 5) control (CT), where KD was performed by injection of short hairpin RNA (shRNA) into marrow cavity; vibration treatment was conducted at 35 Hz, 0.3 g; 20 minutes/day, five days/week). Assessments included radiography, micro-CT, dynamic histomorphometry and immunohistochemistry on DMP1, sclerostin, E11, and fibroblast growth factor 23 (FGF23). In vitro, murine long bone osteocyte-Y4 (MLO-Y4) osteocyte-like cells were randomized as in vivo groupings. DMP1 KD was performed by transfecting cells with shRNA plasmid. Assessments included immunocytochemistry on osteocyte-specific markers as above, and mineralized nodule staining.

### Results

Healing capacities in DMP1 KD groups were impaired. Results showed that DMP1 KD significantly abolished vibration-enhanced fracture healing at week 6. DMP1 KD significantly altered the expression of osteocyte-specific markers. The lower mineralization rate in DMP1 KD groups indicated that DMP1 knockdown was associated with poor fracture healing process.

### Conclusion

The blockage of DMP1 would impair healing outcomes and negate LMHFV-induced enhancement on fracture healing. These findings reveal the importance of DMP1 in response to the mechanical signal during osteoporotic fracture healing.

Cite this article: *Bone Joint Res* 2022;11(7):465–476.

**Keywords:** Osteocyte, Dentin matrix protein 1, Osteoporotic fracture healing, Vibration

Correspondence should be sent to Wing-Hoi Cheung; email: louischeung@cuhk.edu.hk

doi: 10.1302/2046-3758.117.BJR-2021-0476.R2

*Bone Joint Res* 2022;11(7):465–476.

### Article focus

- Osteocytes are mechano-sensors that respond to mechanical stimulation and are suggested to mediate bone formation and resorption.
- Low-magnitude high-frequency vibration (LMHFV) is a non-invasive intervention that has been shown to accelerate osteoporotic fracture healing.

- It is hypothesized that osteocyte-specific dentin matrix protein 1 (DMP1) plays a regulatory role in bone mineralization during LMHFV-accelerated osteoporotic fracture healing.

## Key messages

- Mineralization process was shown to be impaired after knockdown of DMP1 in both in vivo and in vitro models.
- Knockdown of DMP1 altered osteocyte-specific protein expressions, which delayed osteoporotic fracture healing in the metaphyseal fracture model.
- LMHFV-induced enhancement on fracture healing was negated by blockage of DMP1.

## Strengths and limitations

- This is the first study to investigate the role of DMP1 in LMHFV-accelerated osteoporotic fracture healing on a clinically relevant metaphyseal fracture model.
- Both in vivo and in vitro models cannot fully simulate the real clinical situation and further human studies are needed.

## Introduction

Osteoporosis has become a major problem in the ageing population. Osteoporotic patients have an increased risk of fragility fractures; it is estimated that 2 million people suffer from a fragility fracture each year in the USA.[1] Cell metabolism decreases with increasing age, which often impairs healing capacity, leading to prolonged bed-rest and healing times.[2] As a result, the economic burden on fracture care rises annually, with costs at $17.9 billion and £4 billion in the USA and UK, respectively.[3] There is an emerging need for effective therapeutic interventions to accelerate fracture healing.

Low-magnitude high-frequency vibration (LMHFV) is a non-invasive, systemic biophysical intervention that can accelerate osteoporotic fracture healing by enhancing callus formation and mineralization.[4,5] Previous studies also showed that LMHFV improved stem cell recruitment and angiogenesis, which facilitated initiation of fracture healing.[6-8] Recent reports have demonstrated that LMHFV could accelerate fracture healing by enhancing inflammatory response in osteoporotic fracture and fibrinolysis for better vascularization during the healing process.[9-11] All these findings supported LMHFV to be beneficial in accelerating fracture healing.

Osteocytes, which make up 90% of bone cells, are well known for their mechano-sensing function. Studies have shown that osteocytes can facilitate mechanotransduction, which enables them to coordinate activities of osteoblasts and osteoclasts.[12-14] Osteocytes can regulate bone remodelling by altering the production of sclerostin (SOST) and receptor activator of nuclear factor kappaB ligand (RANKL). Bone formation and resorption are adjusted according to the mechanical environment.[15] Moreover, osteogenic and chondrogenic cells are responsive to gravitational force, where the changes in loading condition can contribute to different bone and cartilage pathologies that can affect the fracture healing process.[16,17] A previous study by Cheung et al[18] showed that LMHFV could increase osteocyte numbers and modify their morphology. Vibration therapy can stimulate the formation of osteocyte dendrites in which their extensions are linked to form a widespread lacunocanalicular network (LCN), which increases the sensitivity to mechanical stimulation. Enhanced LCN can facilitate fracture healing as the osteocyte network becomes more capable of transmitting signals and transporting solute molecules.[18-20] However, the underlying mechanism in how these events affect fracture healing is still largely unknown.

Osteocyte-specific proteins are recognized as playing important roles in determining osteocyte maturation and regulating mineralization. E11, known as the early osteocyte marker, is responsible for regulating cell transition from osteoblast to osteocyte.[21] Dentin matrix protein 1 (DMP1) is a glycoprotein that is negatively charged and can be phosphorylated to create more highly negatively charged sites with high affinity for calcium ion binding.[22,23] This also facilitates the nucleation of hydroxyapatite and initiates mineralization during bone formation. DMP1 in osteocytes is responsible for maintenance of LCN and regulation of mineralization.[24,25] They are highly expressed in mature osteocyte dendrites and expression is increased in response to mechanical stimulation.[18,26] Gluhak-Heinrich et al[27] suggested that DMP1 localized along osteocyte dendrites could mediate response to mechanical loading by interacting with actin in the cytoskeleton, which was able to remodel the microenvironment according to loading-induced changes in strain and fluid flow in LCN. Previous studies also reported the importance of DMP1 in fracture healing, especially on the coordination of osteogenesis and osteoclastic bone resorption.[28,29] Fibroblast growth factor 23 (FGF23) is primarily secreted from osteocytes and acts on the kidney,[30,31] and contributes to osteocytes' ability of phosphate homeostasis.[32] SOST secreted from osteocytes is a well-known inhibitor of bone formation by interrupting the Wnt signalling pathway.[33,34] All these factors are mainly found in osteocytes, but their mechanisms in osteoporotic fracture healing are yet to be explored.

Based on current evidence, it was hypothesized that osteocyte-specific DMP1 played a role in LMHFV-augmented osteoporotic fracture healing by altering osteocyte-specific protein expression. This study aimed to investigate the role of osteocyte-specific DMP1 under application of LMHFV in the osteoporotic metaphyseal fracture rat model and in vitro model of murine long bone osteocyte-Y4 (MLO-Y4) osteocyte-like cells.

## Methods

**Study design.** A total of 90 six-month-old female Sprague Dawley rats were obtained with approval from the Animal Experimentation Ethics Committee of The Chinese University of Hong Kong. All rats underwent bilateral

ovariectomy under general anaesthesia and were housed for three additional months for the development of osteoporosis, confirmed by a significant drop in bone mineral density (BMD) at lumbar spine, proximal femur, and distal femur. BMD was measured by dual energy X-ray absorptiometry (DXA; UltraFocus, Faxitron, USA) at pre-ovariectomy (six months) and pre-fracture creation (nine months).

The rats were randomly divided into five groups (n = 6/group/timepoint): vehicle control (CT), vehicle control vibration (VT), DMP1 knockdown (KD), DMP1 knockdown vibration (KD + VT), and Scramble control vibration group (Sb + VT). Rats in vibration groups stood on a bottomless compartmented cage on the vibration platform (V-Health Ltd, Hong Kong) that provided LMHFV at 35 Hz 0.3 g (g = gravitational acceleration). They received treatment 20 minutes/day, five days/week, starting from two days after fracture creation.[6,9,18] Rats in CT and KD groups stood on the vibration platform with power off. Rats were harvested at week 1, 3, and 6 post-fracture. Serial weekly radiographs and micro-CT (μCT) were used to monitor fracture healing progress. Bone mineralization was assessed by dynamic histomorphometry and μCT. Protein expressions across timepoints were assessed by immunohistochemical (IHC) staining.

**Knockdown procedure.** Selected DMP1 shRNA sequence was packaged into adeno-associated virus 9 (AAV9) vector where DMP1-shRNA (targeting 5'-GACCAAAATACTGAATCTGAAA-3'; 5'-TTTCAGATTCAGTATTTTGGTC-3') or scramble control (targeting 5'-GACCATCAATATGACTAGA-3'; 5'-TCTAGTCATCATATTGATGGTC-3') (Division of Life Science, Hong Kong University of Science and Technology (HKUST)) were used. Rats were positioned laterally and a hole was drilled perpendicular to the femoral condyle. A bent needle was used to deliver the AAV9 vector into the marrow cavity.[35] The AAV9 vector ($1 \times 10^{11}$ titer) was injected two weeks before fracture creation, allowing sufficient time for effective knockdown.[36,37]

**Metaphyseal fracture model.** All ovariectomy-induced osteoporotic rats underwent metaphyseal fracture creation according to established protocol.[38,39] A 2.5 cm incision was created along the lateral aspect of the left distal femur, exposing the femur from the femoral condyle to mid-shaft. The patella was dislocated medially to allow better access to the osteotomy site. A six-hole 1 mm T-shaped mini-plate (T-plates, Biortho, China) was used to fix the lateral femur with two 8 mm cortical screws inserted at the distal femoral condyle and three 6 mm screws inserted perpendicular to the femur shaft. An oscillating micro-saw 0.35 mm in width (OT7S-3, Piezosurgery Touch, Metron, Italy) was used to create an osteotomy proximal to the growth plate at the metaphysis. The entire circumference of the bone cortex was cut according to established protocol from previous studies.[9,19,39] The patella was reduced back to position and the wound was closed in layers. Buprenorphine (0.03 mg/kg Temgesic, Schering-Plough, USA) was given postoperatively to reduce pain. Rats with implant failure or signs of pain were euthanized and replaced. All rats were allowed free movement in their cage and ad libitum access to standard rodent diet and water. The procedures adhered to ARRIVE guidelines and an ARRIVE checklist is included in the Supplementary Material.

**Serial radiography.** Healing of the fracture was monitored weekly by lateral radiographs (UltraFocus DXA, Faxitron) taken at an exposure of 40 kVp. All rats were positioned in the same manner for radiographs according to established protocol.[9,19,39] Radiopacity of the metaphyseal osteotomy site was selected and normalized with radiopacity of metal implant. Relative opacity was quantified by image analysis software ImageJ (National Institutes of Health (NIH), USA).

**Micro-CT analysis.** To assess the bone microarchitecture and healing status of the fractured femur, harvested samples were scanned with a μCT system (μCT-40, Scanco Medical, Switzerland). Implants were removed carefully before μCT scan to avoid metal artefacts. The region of interest (ROI) was 1.8 mm above and below the osteotomy site at metaphyseal region. Morphological parameters were evaluated, including tissue volume (TV, $mm^3$), bone volume (BV, $mm^3$), bone volume fraction (BV/TV), BMD (mg HA/ccm), and trabecular thickness (Tb.Th, mm). All assessments were performed according to manufacturer's protocols.

**Dynamic histomorphometry.** The rate of mineralization was assessed by labelling newly formed bone within seven days. Calcein Green (5 mg/kg, MilliporeSigma, USA) and Xylenol Orange (90 mg/kg, MilliporeSigma) were injected two weeks and one week before euthanasia, respectively, to label corresponding newly mineralized surface on day of injection. The fractured left femur bone samples were harvested at week 3 and week 6. After implant removal and μCT scan, samples were dehydrated and embedded in methylmethacrylate (MMA; Technovit 9100, Kulzer, Germany). The samples were sectioned by a saw cutting system (300 CP Contact Point Sawing System, EXAKT, USA), ground, and polished (Phoenix 4000, Buehler, USA) to 100 μm. The newly mineralized surfaces (two weeks and one week before euthanasia) were labelled with green and red fluorescence accordingly (Calcein Green and Xylenol Orange). The fluorescence labels were assessed with ultraviolet fluorescent microscope (DM5500B, Leica, Germany) and mean distance between two lines was measured from the middle of the label lines using analysis software OsteoMeasure Histomorphometry System (OsteoMetrics, USA).

**Immunohistochemistry.** Osteocyte-specific protein expression was evaluated by IHC staining of ROI at cortical region 1 mm above and below the fracture line. Harvested bone samples were fixed in buffered formalin and decalcified with formic acid. They were embedded in paraffin and sectioned at 5 μm thickness using fully automated rotary microtome (RM2255, Leica). IHC staining was performed using horseradish peroxidase/3,3'-diaminobenzidine (HRP/DAB) detection IHC kit (ab64264, Abcam, UK)

following supplier's protocol. The expression of DMP1, SOST, E11, and FGF23 were assessed using anti-DMP1 antibody (LS-B1122650, LifeSpan, USA), anti-SOST antibody (ab63097, Abcam), anti-E11 antibody (bs-1048R, Bioss, USA), and anti-FGF23 antibody (LS-C411984, LifeSpan). The slides were counterstained with haematoxylin and mounted with DPX. Images were obtained using microscopy (DM5500B, Leica) at a magnification of 40×. Positively stained osteocyte numbers were counted to assess for DMP1, E11, and FGF23 expression at four randomly selected sites above and below the fracture gap for each sample.[19] The mean was then calculated. The relative positively stained area was measured for SOST as it was extensively expressed in cluster.[40] ImageJ analysis was performed to quantify the area fraction segmented by colour thresholding.

**MLO-Y4 osteocyte-like cell culture.** MLO-Y4 murine osteocyte-like cell line was cultured on 0.15 mg/ml rat tail type I collagen (A1048301, Thermo Fisher Scientific, USA) coated plates and coverslips. The cells were maintained in alpha-Minimum Essential Medium (αMEM, 11900-024) supplemented with 5% fetal bovine serum (FBS; 10270-106), 5% calf serum (CS, 16010167), and 1% penicillin-streptomycin solution (15640055, all Thermo Fisher Scientific) in a humidified incubator at 5% $CO_2$ and 37°C. Cultured osteocyte-like cells were divided into five groups including CT, VT, KD, KD+VT, and Sb+VT, as in vivo part. The cells in VT groups received 20 minutes/day, five days/week of vibration treatment using a vibration platform providing LMHFV at 35 Hz, 0.3 g.[41-44] Treatment lasted for three, seven, and 14 days before being harvested for assessments including immunocytochemical (ICC) staining and mineralized nodule staining.

**DMP1 knockdown in MLO-Y4 cell line.** In total, $5 \times 10^5$ MLO-Y4 cells were seeded in collagen-coated T-75 flask and transfected with DMP1 shRNA after 80% confluence was reached. Plasmids with DMP1-shRNA (targeting 5'-GACCAAAATACTGAATCTGAAA-3';5'-TTTCAGATTCAGTATTTTGGTC-3') or scramble-shRNA (targeting 5'-GACCATCAATATGACTAGA-3';5'-TCTAGTCATCATATTGATGGTC-3') (Division of Life Science, HKUST) were transfected to MLO-Y4 according to the protocol of Lipofectamine 3000 (L3000015, Thermo Fisher Scientific). Medium was changed after 24 hours of intervention to remove waste and dead cells. Cell culture was expanded until 80% confluence and the cells were trypsinated for seeding further experiment sets. The knockdown efficiency was confirmed by quantitative polymerase chain reaction (qPCR) of extracted RNA from transfected MLO-Y4 cell culture at day 7 according to established protocol using RNAisol Plus (9109, Takara, Japan) and Power SYBR Green PCR Master Mix (4367659, Applied Biosystems, USA). The results were calculated using 2–ΔΔCt method and normalized to glyceraldehyde 3-phosphate dehydrogenase (GAPDH) expression.

**Immunocytochemistry.** Immunocytochemical staining was performed to assess the expression of osteocyte-specific proteins after interventions. MLO-Y4 osteocyte-like cells were seeded on collagen-coated coverslip at $1.5 \times 10^3$ cells/slip and cultured in six-well plates. Cells were harvested at days 3, 7, and 14 for ICC staining of DMP1, SOST, E11, and FGF23. Cells were fixed with 4% paraformaldehyde and cover slips were removed from the well plates. ICC staining was performed using HRP/DAB detection IHC kit following the supplier's protocol with counterstain of haematoxylin. Images were obtained by microscopy, where positively stained area was measured at four randomly selected sites as a mean for each sample. ImageJ analysis was performed to select the areas that were stained brown and quantify the area fraction segmented by colour thresholding relative to ROI. Threshold values of H:50-160, S:0-20, and B:0-200 were used for segmentation, and selected area was quantified as a proportion to the total area of photo.

**Mineralized nodule staining.** MLO-Y4 osteocyte-like cells were seeded on collagen coated six-well plates at $3.5 \times 10^4$ cells/well. The medium was changed to mineralization induction medium (αMEM + 10% FBS + 10 mM β-glycerophosphate (MilliporeSigma) + 50 μg/ml ascorbic acid (MilliporeSigma)) when the culture reached 80% confluence. Cells were harvested and fixed at days 7 and 14, followed by adding 1 ml of 40 mM Alizarin Red S staining (MilliporeSigma) and incubation for 20 minutes. Stained cells were washed and then removed by cell scraper to assess the concentration. Absorbance of samples and their repeats were measured at 405 nm. The results were averaged (mean) and subtracted by the background absorbance.

**Statistical analysis.** All quantitative data were expressed as means (standard deviation (SD)). One-way analysis of variance (ANOVA) with post-hoc Bonferroni multiple comparison tests were performed to analyze the differences among included groups and timepoints. All statistical analyses were performed with SPSS version 26.0 (IBM, USA). Statistical significance was set at $p \leq 0.05$.

## Results

**Confirmation of DMP1 knockdown.** The knockdown of DMP1 could be confirmed because DMP1 expression was decreased and maintained throughout all timepoints, as shown by immunostaining of both localized bone fracture site and MLO-Y4 cell culture model. DMP1 expression in fractured bone of KD group was significantly decreased at weeks 3 and 6 ($p = 0.003$ and $p < 0.001$, respectively). For the in vitro model, a significant decrease of DMP1 expression was found in KD group on days 3 and 7 of MLO-Y4 cell culture ($p = 0.001$ and $p = 0.003$, respectively). Knockdown efficiency of 71.1% was achieved as shown in qPCR results from MLO-Y4 osteocyte-like cells (Supplementary Figure a).

**Serial radiography.** Mean relative radiopacity increased in all groups towards week 6 (Figure 1). Sb + VT group (0.248 (SD 0.056)) had a significantly higher mean radiopacity than KD + VT group (0.169 (SD 0.064)) at week 1 ($p = 0.004$). KD + VT group (0.383 (SD 0.041)) had a significantly lower mean radiopacity than Sb + VT group

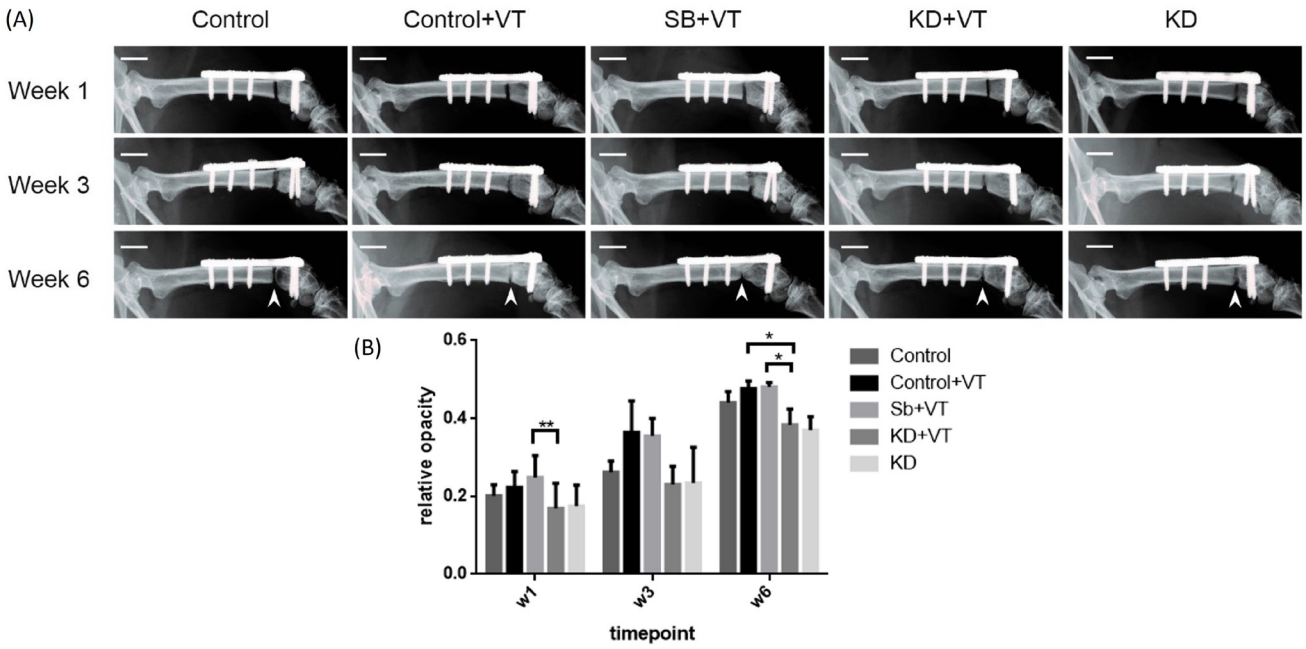


Fig. 1

a) Serial radiography of healing outcome at weeks 1, 3, and 6 post-fracture. Arrowheads indicate the fracture site and the degree of bridging of the gap. Scale bar: 1 mm. b) Relative opacity of all groups at weeks 1, 3, and 6 post-fracture. DMP1 knockdown + vibration (KD + VT) group had a significantly lower radiopacity than Scramble control + vibration (Sb + VT) group at weeks 1 and 6, and significantly lower radiopacity than vibration (VT) group at week 6. Bars represent means (standard deviation), *p ≤ 0.05 and **p ≤ 0.01. Statistical analysis was conducted by one-way analysis of variance with post-hoc Bonferroni tests.

(0.481 (SD 0.011)) and VT group (0.476 (SD 0.02)) at week 6 (p = 0.013 and p = 0.012, respectively). DMP1 knockdown groups generally had lower relative radiopacity than control groups as shown at all timepoints.

**Micro-CT analysis.** The μCT results showed a general improvement of bone microarchitecture in all groups during six weeks of fracture healing. BMD increased gradually in all groups, reaching the highest level at week 6. Tissue volume of the VT and Sb + VT group was significantly higher than that of the KD + VT group (p = 0.012 and p = 0.007, respectively) at week 1. For bone volume, knockdown groups had less bone at weeks 3 and 6 compared with the VT and Sb + VT groups, whereas the KD + VT group had significantly lower bone volume than Sb + VT group at week 3 (p = 0.010). There was an increasing trend of bone volume fraction across the timepoints in all groups, but the percentage change in knockdown groups (17%) was lower than those of the other two vibration groups (30%). Bone volume fraction of Sb + VT group was significantly higher than that of KD + VT group (p = 0.034) at week 3. For trabecular thickness, Sb + VT group was significantly higher than KD + VT group at week 3 (p = 0.021) (Figure 2).

**Dynamic histomorphometry.** Mineralization was found towards the end of the healing process, where mineral apposition rate (MAR) reached the highest level at week 6 post-fracture (Figure 3). Knockdown groups showed decreased MAR at all timepoints, in which the KD + VT group had significantly lower MAR than the VT group (p = 0.036) at week 6. Also, the thicker fluorescence label lines in VT and Sb + VT groups demonstrated higher amounts of mineral accumulation on these bone surfaces.

**Immunohistochemistry.** DMP1 expression of knockdown groups remained at a low level across all timepoints (Figure 4b). CT, VT, and Sb + VT groups showed steady increase of DMP1 towards week 6, where a significant difference was reached between CT group and KD group (p = 0.033). VT group had significantly higher DMP1 expression than KD + VT group at both week 3 and week 6 (p = 0.008 and p < 0.001, respectively). A significant difference was also found between Sb + VT and KD + VT groups at week 6 (p = 0.030).

The expression of SOST in knockdown groups was higher at all timepoints compared to the other three groups (Figure 4c). Vibration groups generally had lower SOST expression but the KD + VT group had an opposite result, for which this expression was significantly higher than VT and Sb + VT groups (p = 0.001, and p = 0.007, respectively) at week 6.

There was a decreasing trend of E11 expression among all groups towards the end of the healing process at week 6 post-fracture (Figure 4d). The KD group had significantly higher E11 expression than the CT group at week 1 (p = 0.050). The KD + VT group also showed significantly increased expression of E11 compared with the Sb + VT group at both week 1 and week 3 (p = 0.024 and p = 0.008, respectively) and the VT group at week 3 (p = 0.048).

The expression of FGF23 followed an increasing trend towards week 3 and decreased at week 6 (Figure 4e). The

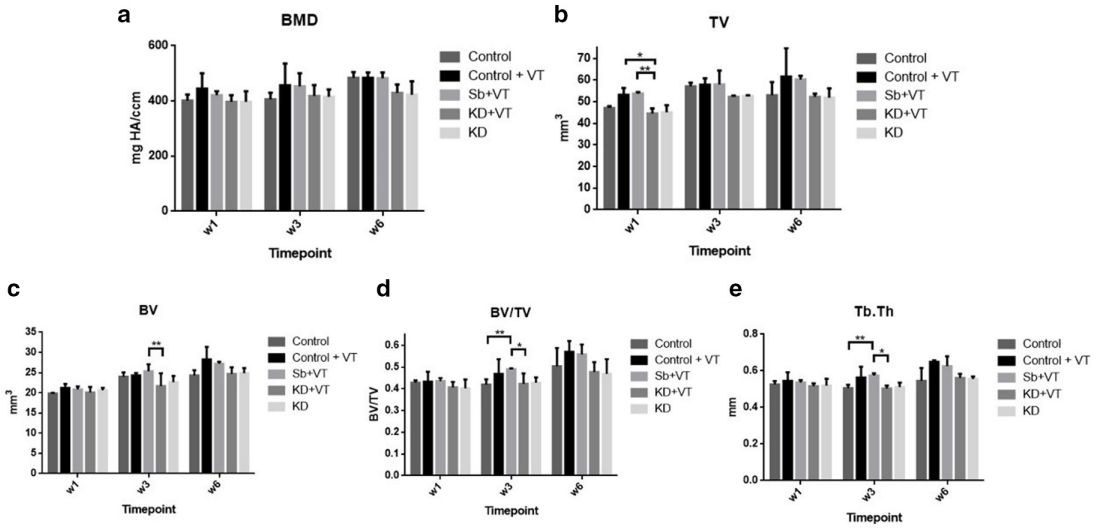


Fig. 2

Parameters assessed in micro-CT analysis at weeks 1, 3, and 6 post-fracture. a) Increasing bone mineral density (BMD) towards fracture healing. b) Tissue volume (TV) in DMP1 knockdown + vibration (KD + VT) group was significantly decreased compared to vibration (VT) and Scramble control + vibration (Sb + VT) groups at week 1. c) Bone volume (BV) was comparatively lower in knockdown groups and a significant difference was recorded between KD + VT group and Sb+ VT group at week 3. d) Bone volume fraction (BV/TV) increased steadily toward week 6. Significant difference was recorded at week 3 in Sb + VT compared to KD + VT. e) Trabecular thickness (Tb.Th) of KD + VT group was significantly lower than that of Sb + VT group at week 3. Bars represent means (standard deviation), *p ≤ 0.05 and **p ≤ 0.01. Statistical analysis was conducted by one-way analysis of variance with post-hoc Bonferroni tests.

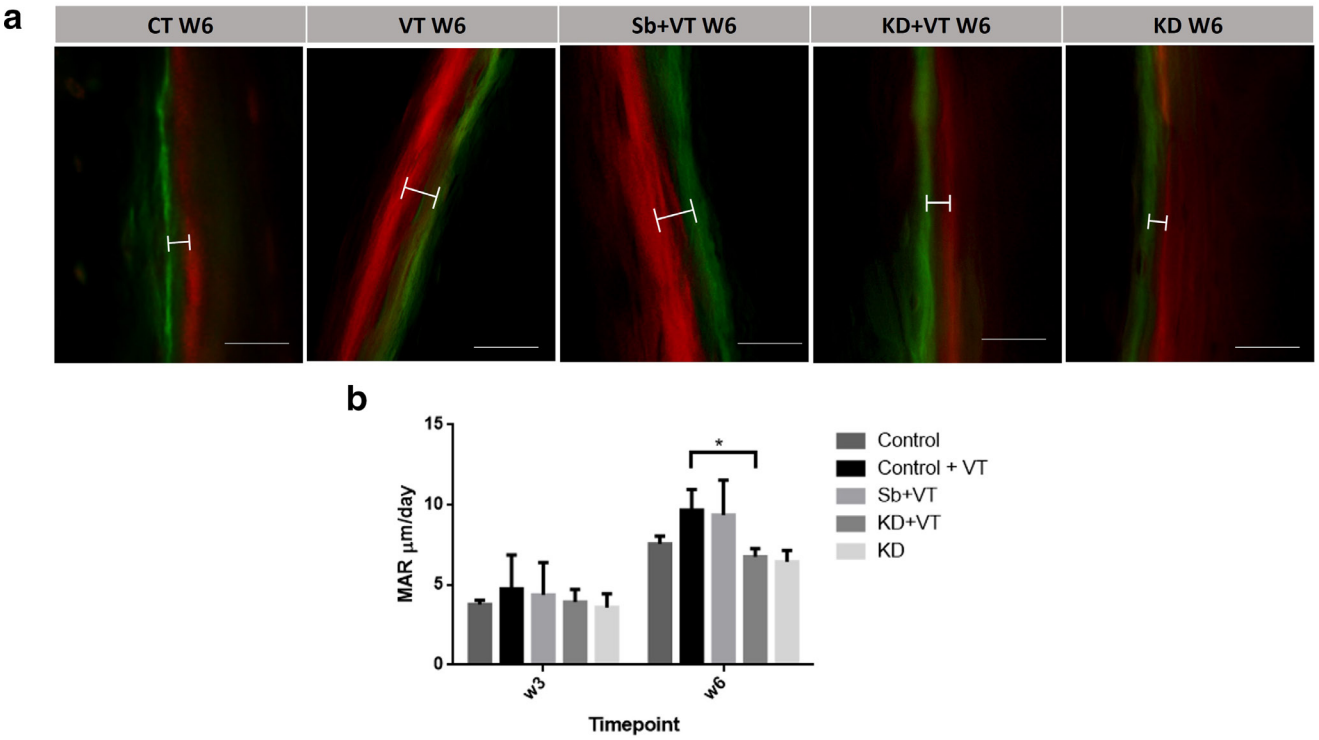


Fig. 3

a) Mineral apposition rate (MAR) at week 6 post-fracture, where the mean distance between the lines of mineral deposition (green fluorescence and red fluorescence labels with Calcein Green and Xylenol Orange, respectively) was measured. Magnification: 20×, scale bar: 25 µm. b) Knockdown groups had significantly lower MAR at week 6. Bars represent means (standard deviation), *p ≤ 0.05. Statistical analysis was conducted by one-way analysis of variance with post-hoc Bonferroni tests. KD, knockdown; Sb, Scramble; VT, vibration.

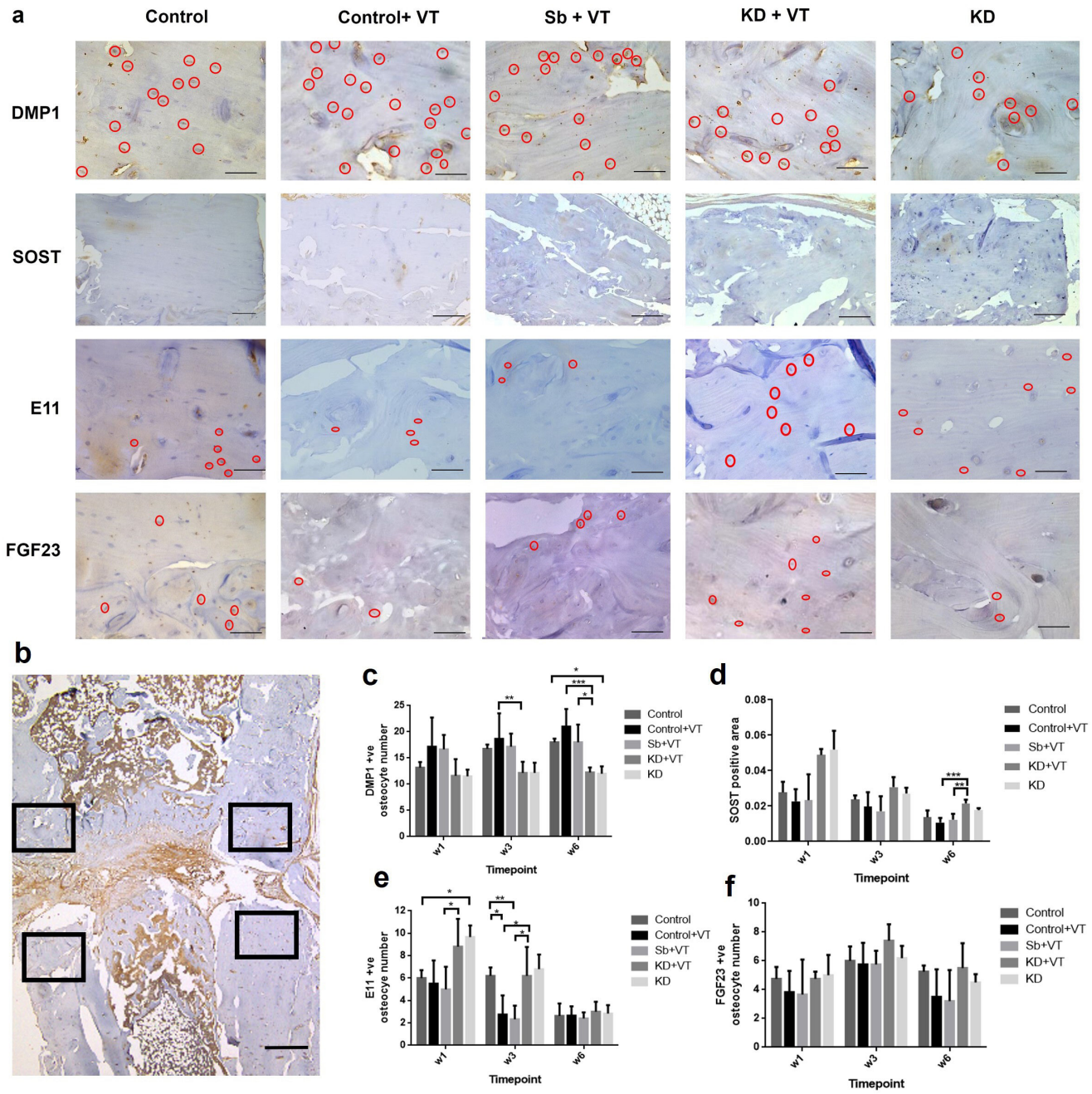


Fig. 4

a) Immunohistochemical staining of osteocyte-specific proteins at their corresponding significantly expressed timepoints (dentin matrix protein 1 (DMP1) and sclerostin (SOST) expression at week 6, E11, and fibroblast growth factor 23 (FGF23) expression at week 3). Magnification: 40×, scale bar: 50 µm. b) Representative image of the overall view of bone sample showing the region of interest (ROI) for quantification of positive signals, produced by immunohistochemical staining. Four sites were selected for measurement. Magnification: 2.5×, scale bar: 500 µm. c) Significantly decreased DMP1-positive osteocytes in DMP1 knockdown (KD) groups showed successful knockdown of DMP1 and consistency throughout the healing period. d) Vibration induced suppression of SOST was not seen in knockdown (KD) groups. SOST expression was significantly higher in DMP1 KD + vibration (KD + VT) group than VT and Scramble control + VT (Sb + VT) groups at week 6. e) E11 expression in DMP1 KD + VT group was significantly higher than Sb + VT group at both week 1 and week 3, indicating delayed fracture healing as E11 was pre-osteocyte formed during the healing process. f) FGF23 expression increased at week 3 and decreased at week 6. FGF23 expression in osteocytes was elevated with the knockdown of DMP1. Bars represent means (standard deviation), *p ≤ 0.05, **p ≤ 0.01, and ***p ≤ 0.001. Statistical analysis was conducted by one-way analysis of variance with post-hoc Bonferroni tests.

KD groups had comparatively higher FGF23 expression at all time points compared to the other groups. Vibration treatment had reduced the FGF23 expression in VT and Sb + VT groups compared to CT group, but this reduction was not found in the KD + VT group.

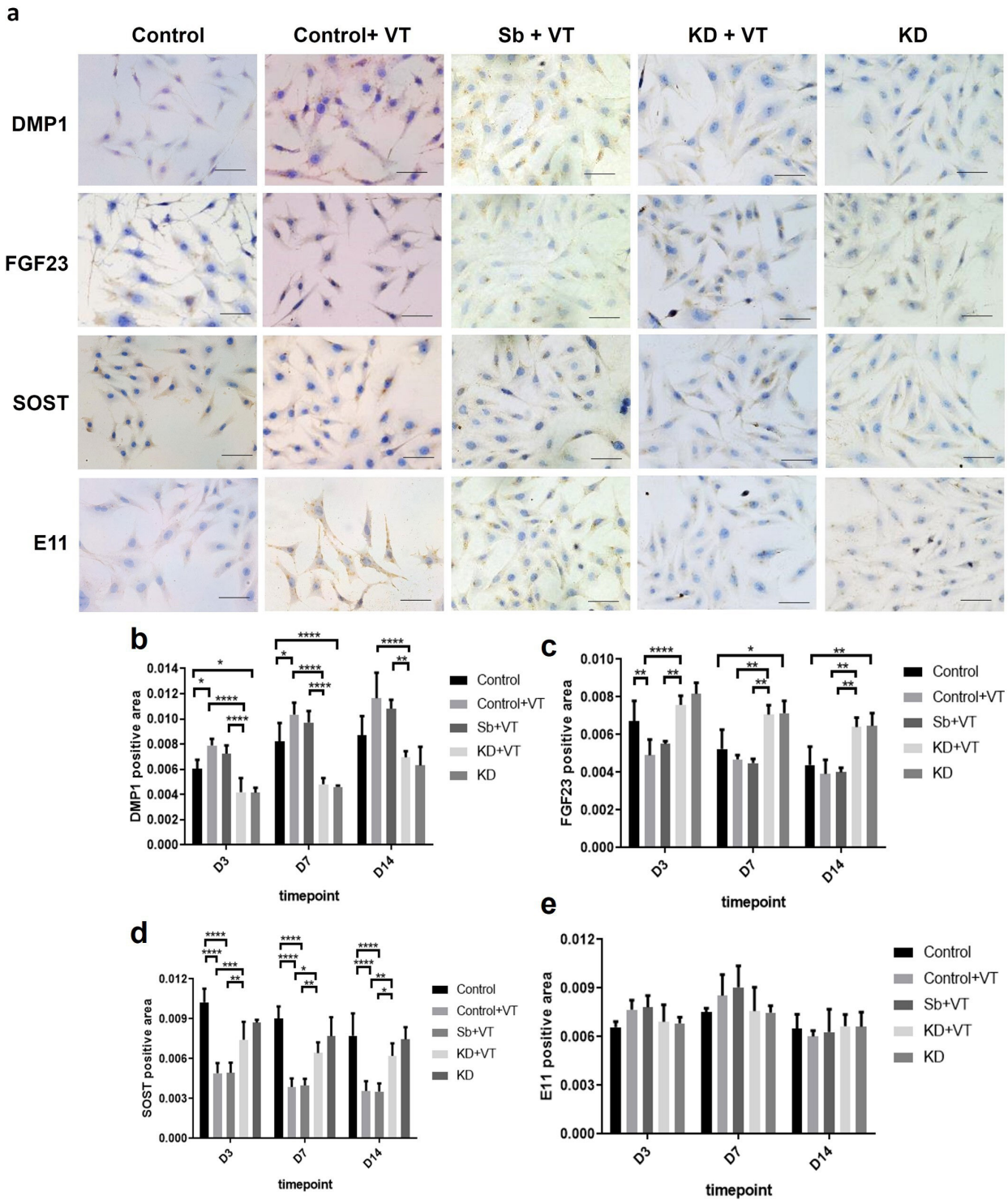


Fig. 5

a) Representative images of immunocytochemical staining of osteocyte-specific proteins in murine long bone osteocyte-Y4 (MLO-Y4) cell culture at Day 7. Osteocytes in brown indicate a positive signal. Magnification: 40×, scale bar: 50 µm. b) Vibration significantly increased dentin matrix protein 1 (DMP1) expression and knockdown had negated vibration effect. c) DMP1 knockdown + vibration (KD + VT) group had significantly higher fibroblast growth factor 23 (FGF23) positive osteocytes than vibration (VT) and Scramble control + vibration (Sb + VT) groups at all timepoints. Vibration reduced FGF23 expression at all timepoints as DMP1 expression was increased after vibration. d) Sclerostin (SOST) expression was significantly suppressed by vibration at all timepoints. KD + VT group had significantly higher SOST expression than VT and Sb + VT groups at all timepoints as vibration effect was abrogated by DMP1 KD. e) E11 expression in MLO-Y4 culture increased at day 7 and decreased at day 14. The number of pre-osteocytes was increasing but later decreased as the culture reached its confluency. Bars represent means (standard deviation), *p ≤ 0.05, **p ≤ 0.01, ***p ≤ 0.001, and ****p ≤ 0.0001. Statistical analysis was conducted by one-way analysis of variance with post-hoc Bonferroni tests.

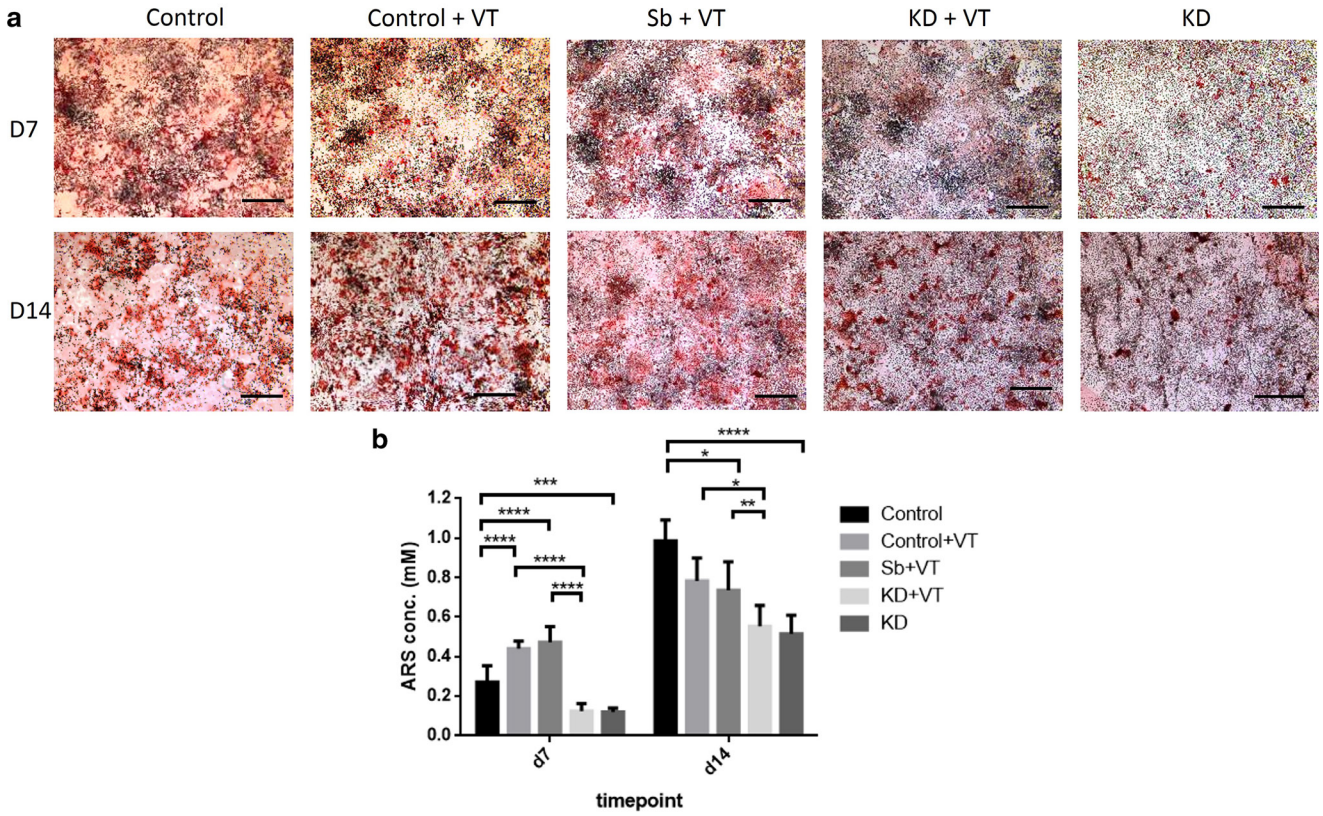


Fig. 6

a) Staining of mineralized nodules at day 7 and day 14 of murine long bone osteocyte-Y4 (MLO-Y4) culture. Positive signals were stained red. Magnification 2.5×, scale bar: 1 mm. b) Dentin matrix protein 1 (DMP1) knockdown (KD) reduced mineralization as the mineralized nodules in DMP1 KD + vibration (KD + VT) were significantly lower compared to VT and Scramble control + VT (Sb + VT) groups. Vibration enhancement on mineralization was also negated by DMP1 KD. Bars represent means (standard deviation), *p ≤ 0.05, **p ≤ 0.01, ***p ≤ 0.001, and ****p ≤ 0.0001. Statistical analysis was conducted by one-way analysis of variance with post-hoc Bonferroni tests.

**Immunocytochemistry.** Osteocyte-specific protein expression in MLO-Y4 culture was assessed by ICC staining (Figure 5a). There was an increasing trend of DMP1 expression in all groups across all timepoints and this reached the highest level on day 14 (Figure 5b). The VT and Sb + VT groups significantly enhanced the expression of DMP1 on day 3 and day 7 of cell culture compared with the CT group ($p = 0.033$ and $p = 0.025$, respectively). The KD group significantly reduced DMP1 expression on day 3 and day 7 ($p = 0.012$ and $p < 0.001$, respectively) compared with the CT group. The expression of DMP1 in the KD + VT group was significantly decreased compared to the VT and Sb + VT groups at all timepoints (day 3: $p < 0.001$ for both groups; day 7: $p < 0.001$ for both groups; day 14: $p < 0.001$ and $p = 0.005$, respectively).

The expression of FGF23 decreased steadily across all timepoints (Figure 5c). VT group significantly reduced FGF23 expression when compared to CT group ($p = 0.009$) on day 3. The expression of FGF23 in KD group was significantly increased compared to CT group on both day 7 and day 14 ($p = 0.025$ and $p = 0.008$, respectively). The expression of FGF23 in KD + VT group was significantly increased compared to VT and Sb + VT groups at all timepoints (day 3: $p < 0.001$ and $p = 0.007$; day 7: $p = 0.004$ and $p = 0.002$; day 14: $p = 0.002$ and $p = 0.018$, respectively).

There was a gradual decline in SOST expression towards 14 days of culture (Figure 5d). The expression of SOST in VT and Sb + VT groups remained at a low level compared to the other three groups. CT group had significantly higher SOST expression at all time points compared to VT and Sb + VT groups ($p < 0.001$ for both groups). The expression of SOST in KD + VT group was significantly higher than those of VT and Sb + VT groups at all timepoints (day 3: $p = 0.006$ and $p = 0.007$; day 7: $p = 0.013$ and $p = 0.008$; day 14: $p = 0.010$ and $p = 0.013$, respectively).

E11 expression level fluctuated within a small range across the timepoints, where it reached the highest level on day 7 and decreased on day 14 (Figure 5e). VT and Sb + VT groups generally showed increased E11 expression compared with the CT group. Knockdown groups had a relatively lower level of expression of E11. There was no significant difference among groups across all timepoints.

**Mineralized nodule staining.** In general, all experimental groups showed elevated mineralized nodules on day 14 compared to day 7 (Figure 6). The mineralized nodules in the KD group were significantly reduced compared to

the CT group on both day 7 and day 14 ($p = 0.001$ and $p < 0.001$, respectively). Vibration treatment significantly increased mineralization in VT and Sb + VT groups compared to CT group on day 7 ($p < 0.001$ for both groups). The mineralized nodules in KD + VT group was significantly decreased compared to VT and Sb + VT groups at both timepoints (day 7: $p < 0.001$ for both groups; day 14: $p = 0.017$ and $p = 0.002$, respectively).

## Discussion

This study investigated the role of osteocyte-specific DMP1 in LMHFV enhanced osteoporotic fracture healing through evaluating the healing capacity and changes in osteocyte-specific protein expression after the knockdown of DMP1. In this study, in vivo results demonstrated that DMP1 knockdown could impair fracture healing by altering the expression of different osteocyte-specific proteins and interrupting the mineralization process. Additionally, the vibration effect on accelerating fracture healing was negated by the blockage of DMP1. In vitro results also showed a similar trend of protein expression changes and the impairment of mineralization after knockdown of DMP1 in osteocyte-like cell culture. Taken together, osteocyte-specific DMP1 played an important role in regulating mineralization and also in mediating LMHFV-augmented osteoporotic fracture healing.

Various studies had demonstrated that vibration treatment could accelerate osteoporotic fracture healing and facilitate positive changes in osteocyte-specific protein expression. The increase in relative radiopacity after LMHFV indicated more tissue growth and bone remodelling at the fracture site, which were substantiated by previous studies.[9,18] The elevated DMP1 expression after vibration treatment implied an increase in osteocyte number and elongation of osteocyte dendrites. As DMP1 is highly expressed in mature osteocyte dendrites and is responsible for regulation of mineralization, the higher mineral apposition rate in the VT group compared to the CT group had again proved the positive effect of vibration on acceleration of the healing process. Our results also demonstrated the suppression of SOST after application of mechanical loading, which was consistent with previous studies.[18,45] Fracture healing was accelerated under the inhibition of SOST, which could activate the Wnt/β catenin pathway and promote bone formation.[46-48]

In order to investigate the role of osteocyte-specific DMP1 in osteoporotic fracture healing, DMP1 knockdown was performed in both animal model and in vitro model. Both results showed undesirable mineralization outcomes, including the reduction in rate and amount of mineral deposition. As the phosphorylated C terminal fragment of DMP1 could work as a nucleator of hydroxyapatite crystals, knocking down DMP1 would reduce the targets for hydroxyapatite nucleation and impede the initiation of mineralization.[25,49] Healing activities were impaired in the knockdown group, and provision of LMHFV could not rescue the healing process. There was no significant difference found in all assessments when comparing DMP1 knockdown group with and without vibration. These observations confirmed that vibration-induced increase in mineralization was negated by the knockdown of DMP1. As the KD + VT group was significantly different from the VT group in terms of radiopacity, mineralization rate, and protein expression, blockage of DMP1 was proven to cause delayed osteoporotic fracture healing. Besides, our in vivo results demonstrated an increase in E11 expression in DMP1 knockdown groups, which indicated a comparatively slower healing process where pre-osteocytes were still transiting from osteoblasts and fewer DMP1-expressing mature osteocytes were formed.[21]

To our knowledge, this is the first study to investigate the role of osteocyte-specific DMP1 in LMHFV enhanced osteoporotic fracture healing by knockdown of DMP1 in a rat metaphyseal fracture model. There have been several studies which used the DMP1-null mice model, but these mainly focused on mineral metabolism and phosphate homeostasis.[24,50-52] Hypophosphatemia and osteomalacia are common with the loss of DMP1. These phenotypes are mainly caused by phosphate imbalance and defective maturation of osteocytes.[50,51] DMP1 is essential in maintenance of osteocyte LCN, and mineralization is impaired due to the disorientated LCN matrix.[24] In consideration of the LCN modelling process, vibration treatment could enhance mechanosensing ability and signal transmission in osteocyte network, which could later affect the healing capacity by regulating mineralization.[18,19] The knockdown of DMP1 led to defective osteocytes and impairment in mechanosensing ability. Our study provides an insight into the critical regulatory role of DMP1 in the relationship between vibration treatment and osteoporotic fracture healing. Our results also confirmed that loss of DMP1 would weaken healing performance, i.e. the bridging of fracture gap and bone microarchitecture.

Apart from maintenance of LCN and direct regulation of mineralization, DMP1 is also a negative regulator of FGF23.[25] Elevated expression of FGF23 was extensively reported from previous studies using the DMP1-null mice model.[24,50,51] Increased level of FGF23 could inhibit active vitamin D synthesis and phosphate reabsorption in the kidney.[30,32,51,53] Both our in vivo and in vitro results were consistent with previous studies' findings that knockdown of DMP1 resulted in elevated FGF23 expression. A defective mineralization process was also observed in our findings. FGF23 was associated with renal phosphate wasting, which resulted in a low serum phosphate level and the availability of free phosphate was thus greatly hindered.[31,54] As phosphate is one of the components of the bone matrix, insufficiency of free phosphate would delay mineralization.[55] Furthermore, both our in vivo and in vitro results demonstrated an increase in SOST expression after knockdown of DMP1. Previous studies have found that increased SOST could result in elevated matrix extracellular phosphoglycoprotein (MEPE) expression. The acidic serine aspartate-rich MEPE-associated motif

(ASARM) of MEPE was reported to interrupt mineralization by binding to hydroxyapatite crystal and thereby preventing nucleation.[54,56,57] These findings suggested that DMP1 not only regulates mineralization by altering FGF23 expression and kidney reabsorption, but also affects the presence of ASARM and hydroxyapatite crystal nucleation.

The limitation of this study is that the rat model cannot fully simulate real situations of bone healing in humans, as the two species have different metabolic rates. Furthermore, as rats are quadrupedal and humans are bipedal, the transmission of vibration force is different. Moreover, the animal model employed was not a complete knockout of DMP1 where remnant effect of DMP1 could be observed. Complete knockout can be done in mice models, but osteoporotic fracture creation at the metaphyseal region is technically demanding in mice. Furthermore, the metabolic pathways in humans are complicated and interdependent. There are many mechanisms that can affect the bone healing process including osteogenesis, inflammatory response, and macrophage polarization. The pathways involved in osteogenesis and osteoimmunology may be related to osteocyte function and DMP1 mechanism, and further investigations are needed to delineate this relationship.[58-61] Also, microRNAs and gut microbiota contribute to homeostasis of the musculoskeletal system, and studies have reported that they affect BMD and facilitate fracture healing; further studies may investigate their relationship with osteocytes and their role in healing.[62-66]

In conclusion, our results showed impaired mineralization and fracture healing after the knockdown of DMP1. This study has demonstrated the important role of DMP1 in LMHFV enhanced osteoporotic fracture healing by altering osteocyte-specific protein expression. Moreover, there are multiple pathways which contribute to regulating mineralization, including FGF23-mediated phosphate homeostasis in the kidney and SOST-associated regulation of mineralization. Further studies are required to delineate the mechanism behind the complicated regulatory role of DMP1. Through a better understanding of the DMP1 mechanism in mineralization, new therapeutic drugs can be developed to treat osteoporotic fracture patients.

## Supplementary material

Figure displaying dentin matrix protein 1 knockdown efficiency, and an ARRIVE checklist showing that the ARRIVE guidelines were adhered to in this study.

## References


1. **Ensrud KE**. Epidemiology of fracture risk with advancing age. *J Gerontol A Biol Sci Med Sci*. 2013;68(10):1236–1242.
2. **Cheung WH**, **Miclau T**, **Chow SKH**, **Yang FF**, **Alt V**. Fracture healing in osteoporotic bone. *Injury*. 2016;47 Suppl 2:S21-6.
3. **Clynes MA**, **Harvey NC**, **Curtis EM**, **Fuggle NR**, **Dennison EM**, **Cooper C**. The epidemiology of osteoporosis. *Br Med Bull*. 2020;133(1):105–117.
4. **Chow DHK**, **Leung KS**, **Qin L**, **Leung AHC**, **Cheung WH**. Low-magnitude high-frequency vibration (LMHFV) enhances bone remodeling in osteoporotic rat femoral fracture healing. *J Orthop Res*. 2011;29(5):746–752.
5. **Chow SKH**, **Leung KS**, **Qin J**, **et al**. Mechanical stimulation enhanced estrogen receptor expression and callus formation in diaphyseal long bone fracture healing in ovariectomy-induced osteoporotic rats. *Osteoporos Int*. 2016;27(10):2989–3000.
6. **Shi HF**, **Cheung WH**, **Qin L**, **Leung AHC**, **Leung KS**. Low-magnitude high-frequency vibration treatment augments fracture healing in ovariectomy-induced osteoporotic bone. *Bone*. 2010;46(5):1299–1305.
7. **Cheung W-H**, **Sun M-H**, **Zheng Y-P**, **et al**. Stimulated angiogenesis for fracture healing augmented by low-magnitude, high-frequency vibration in a rat model-evaluation of pulsed-wave doppler, 3-D power Doppler ultrasonography and micro-CT microangiography. *Ultrasound Med Biol*. 2012;38(12):2120–2129.
8. **Wei FY**, **Chow SK**, **Leung KS**, **et al**. Low-magnitude high-frequency vibration enhanced mesenchymal stem cell recruitment in osteoporotic fracture healing through the SDF-1/CXCR4 pathway. *Eur Cell Mater*. 2016;31:341–354.
9. **Wong RMY**, **Choy VMH**, **Li J**, **et al**. Fibrinolysis as a target to enhance osteoporotic fracture healing by vibration therapy in a metaphyseal fracture model. *Bone Joint Res*. 2021;10(1):41–50.
10. **Chow SK-H**, **Chim Y-N**, **Wang J**, **et al**. Vibration treatment modulates macrophage polarisation and enhances early inflammatory response in oestrogen-deficient osteoporotic-fracture healing. *Eur Cell Mater*. 2019;38:228–245.
11. **Chow SK-H**, **Chim Y-N**, **Wang J-Y**, **Wong RM-Y**, **Choy VM-H**, **Cheung W-H**. Inflammatory response in postmenopausal osteoporotic fracture healing. *Bone Joint Res*. 2020;9(7):368–385.
12. **Li MCM**, **Chow SKH**, **Wong RMY**, **Qin L**, **Cheung WH**. The role of osteocytes-specific molecular mechanism in regulation of mechanotransduction - A systematic review. *J Orthop Translat*. 2021;29:1–9.
13. **Hemmatian H**, **Bakker AD**, **Klein-Nulend J**, **van Lenthe GH**. Aging, osteocytes, and mechanotransduction. *Curr Osteoporos Rep*. 2017;15(5):401–411.
14. **Stewart S**, **Darwood A**, **Masouros S**, **Higgins C**, **Ramasamy A**. Mechanotransduction in osteogenesis. *Bone Joint Res*. 2020;9(1):1–14.
15. **Dallas SL**, **Prideaux M**, **Bonewald LF**. The osteocyte: an endocrine cell… and more. *Endocr Rev*. 2013;34(5):658–690.
16. **Ali E**, **Birch M**, **Hopper N**, **Rushton N**, **McCaskie AW**, **Brooks RA**. Human osteoblasts obtained from distinct periarticular sites demonstrate differences in biological function in vitro. *Bone Joint Res*. 2021;10(9):611–618.
17. **Lawrence EA**, **Aggleton J**, **van Loon J**, **et al**. Exposure to hypergravity during zebrafish development alters cartilage material properties and strain distribution. *Bone Joint Res*. 2021;10(2):137–148.
18. **Cheung WH**, **Wong RMY**, **Choy VMH**, **Li MCM**, **Cheng KYK**, **Chow SKH**. Enhancement of osteoporotic fracture healing by vibration treatment: The role of osteocytes. *Injury*. 2021;52 Suppl 2:S97–S100.
19. **Choy M-HV**, **Wong RM-Y**, **Li M-C**, **et al**. Can we enhance osteoporotic metaphyseal fracture healing through enhancing ultrastructural and functional changes of osteocytes in cortical bone with low-magnitude high-frequency vibration? *FASEB J*. 2020;34(3):4234–4252.
20. **Choy MHV**, **Wong RMY**, **Chow SKH**, **et al**. How much do we know about the role of osteocytes in different phases of fracture healing? A systematic review. *J Orthop Translat*. 2020;21:111–121.
21. **Staines KA**, **Prideaux M**, **Allen S**, **Buttle DJ**, **Pitsillides AA**, **Farquharson C**. E11/podoplanin protein stabilization through inhibition of the proteasome promotes osteocyte differentiation in murine in vitro models. *J Cell Physiol*. 2016;231(6):1392–1404.
22. **Rios HF**, **Ye L**, **Dusevich V**, **Eick D**, **Bonewald LF**, **Feng JQ**. DMP1 is essential for osteocyte formation and function. *J Musculoskelet Neuronal Interact*. 2005;5(4):325–327.
23. **Narayanan K**, **Ramachandran A**, **Hao J**, **et al**. Dual functional roles of dentin matrix protein 1. Implications in biomineralization and gene transcription by activation of intracellular Ca2+ store. *J Biol Chem*. 2003;278(19):17500–17508.
24. **Feng JQ**, **Ward LM**, **Liu S**, **et al**. Loss of DMP1 causes rickets and osteomalacia and identifies a role for osteocytes in mineral metabolism. *Nat Genet*. 2006;38(11):1310–1315.
25. **Lu Y**, **Yuan B**, **Qin C**, **et al**. The biological function of DMP-1 in osteocyte maturation is mediated by its 57-kDa C-terminal fragment. *J Bone Miner Res*. 2011;26(2):331–340.
26. **Harris SE**, **Gluhak-Heinrich J**, **Harris MA**, **et al**. DMP1 and MEPE expression are elevated in osteocytes after mechanical loading *in vivo*: theoretical role in controlling mineral quality in the perilacunar matrix. *J Musculoskelet Neuronal Interact*. 2007;7(4):313–315.

27. **Gluhak-Heinrich J**, **Ye L**, **Bonewald LF**, **et al**. Mechanical loading stimulates dentin matrix protein 1 (DMP1) expression in osteocytes in vivo. *J Bone Miner Res*. 2003;18(5):807–817.
28. **Toyosawa S**, **Kanatani N**, **Shintani S**, **et al**. Expression of dentin matrix protein 1 (DMP1) during fracture healing. *Bone*. 2004;35(2):553–561.
29. **Sun Y**, **Weng Y**, **Zhang C**, **et al**. Glycosylation of dentin matrix protein 1 is critical for osteogenesis. *Sci Rep*. 2015;5:17518.
30. **Hu MC**, **Shi MJ**, **Moe OW**. Role of αKlotho and FGF23 in regulation of type II Na-dependent phosphate co-transporters. *Pflugers Arch*. 2019;471(1):99–108.
31. **Rowe PSN**. Regulation of bone-renal mineral and energy metabolism: the PHEX, FGF23, DMP1, MEPE ASARM pathway. *Crit Rev Eukaryot Gene Expr*. 2012;22(1):61–86.
32. **Feng JQ**, **Ye L**, **Schiavi S**. Do osteocytes contribute to phosphate homeostasis? *Curr Opin Nephrol Hypertens*. 2009;18(4):285–291.
33. **Burgers TA**, **Williams BO**. Regulation of Wnt/β-catenin signaling within and from osteocytes. *Bone*. 2013;54(2):244–249.
34. **Spatz JM**, **Wein MN**, **Gooi JH**, **et al**. The Wnt inhibitor sclerostin is up-regulated by mechanical unloading in osteocytes in vitro. *J Biol Chem*. 2015;290(27):16744–16758.
35. **Zhang Y**, **Xu J**, **Ruan YC**, **et al**. Implant-derived magnesium induces local neuronal production of CGRP to improve bone-fracture healing in rats. *Nat Med*. 2016;22(10):1160–1169.
36. **Lee LR**, **Peacock L**, **Lisowski L**, **Little DG**, **Munns CF**, **Schindeler A**. Targeting adeno-associated virus vectors for local delivery to fractures and systemic delivery to the skeleton. *Mol Ther Methods Clin Dev*. 2019;15:101–111.
37. **Yuasa M**, **Mignemi NA**, **Nyman JS**, **et al**. Fibrinolysis is essential for fracture repair and prevention of heterotopic ossification. *J Clin Invest*. 2015;125(8):3117–3131.
38. **Wong RMY**, **Choy MHV**, **Li MCM**, **et al**. A systematic review of current osteoporotic metaphyseal fracture animal models. *Bone Joint Res*. 2018;7(1):6–11.
39. **Wong RM**, **Thormann U**, **Choy MH**, **et al**. A metaphyseal fracture rat model for mechanistic studies of osteoporotic bone healing. *Eur Cell Mater*. 2019;37:420–430.
40. **Barbe MF**, **Massicotte VS**, **Assari S**, **et al**. Prolonged high force high repetition pulling induces osteocyte apoptosis and trabecular bone loss in distal radius, while low force high repetition pulling induces bone anabolism. *Bone*. 2018;110:267–283.
41. **Zhang N**, **Chim YN**, **Wang J**, **Wong RMY**, **Chow SKH**, **Cheung WH**. Impaired fracture healing in sarco-osteoporotic mice can be rescued by vibration treatment through myostatin suppression. *J Orthop Res*. 2020;38(2):277–287.
42. **Marycz K**, **Lewandowski D**, **Tomaszewski KA**, **Henry BM**, **Golec EB**, **Marędziak M**. Low-frequency, low-magnitude vibrations (LFLM) enhances chondrogenic differentiation potential of human adipose derived mesenchymal stromal stem cells (hASCs. *PeerJ*. 2016;4:e1637.
43. **Leung KS**, **Li CY**, **Tse YK**, **et al**. Effects of 18-month low-magnitude high-frequency vibration on fall rate and fracture risks in 710 community elderly--a cluster-randomized controlled trial. *Osteoporos Int*. 2014;25(6):1785–1795.
44. **Chow SKH**, **Cui C**, **Cheng KYK**, **et al**. Acute inflammatory response in osteoporotic fracture healing augmented with mechanical stimulation is regulated in vivo through the p38-MAPK pathway. *Int J Mol Sci*. 2021;22(16):8720.
45. **Koide M**, **Kobayashi Y**. Regulatory mechanisms of sclerostin expression during bone remodeling. *J Bone Miner Metab*. 2019;37(1):9–17.
46. **Suen PK**, **Qin L**. Sclerostin, an emerging therapeutic target for treating osteoporosis and osteoporotic fracture: A general review. *J Orthop Translat*. 2016;4:1–13.
47. **Robling AG**, **Niziolek PJ**, **Baldridge LA**, **et al**. Mechanical stimulation of bone in vivo reduces osteocyte expression of Sost/sclerostin. *J Biol Chem*. 2008;283(9):5866–5875.
48. **Lara-Castillo N**, **Kim-Weroha NA**, **Kamel MA**, **et al**. In vivo mechanical loading rapidly activates β-catenin signaling in osteocytes through a prostaglandin mediated mechanism. *Bone*. 2015;76:58–66.
49. **Lin S**, **Zhang Q**, **Cao Z**, **et al**. Constitutive nuclear expression of dentin matrix protein 1 fails to rescue the Dmp1-null phenotype. *J Biol Chem*. 2014;289(31):21533–21543.
50. **Liu SG**, **Zhou JP**, **Tang W**, **Menard R**, **Feng JQ**, **Quarles LD**. Pathogenic role of Fgf23 in Dmp1-null mice. *Am J Physiol Endocrinol Metab*. 2008;295(2):E254-61.
51. **Ichikawa S**, **Gerard-O'Riley RL**, **Acton D**, **et al**. A mutation in the Dmp1 gene alters phosphate responsiveness in mice. *Endocrinology*. 2017;158(3):470–476.
52. **Zhang Q**, **Lin SX**, **Liu Y**, **Yuan BZ**, **Harris SE**, **Feng JQ**. Dmp1 null mice develop a unique osteoarthritis-like phenotype. *Int J Biol Sci*. 2016;12(10):1203–1212.
53. **Gohil A**, **Imel EA**. FGF23 and associated disorders of phosphate wasting. *Pediatr Endocrinol Rev*. 2019;17(1):17–34.
54. **Quarles LD**. FGF23, PHEX, and MEPE regulation of phosphate homeostasis and skeletal mineralization. *Am J Physiol Endocrinol Metab*. 2003;285(1):E1-9.
55. **Goretti Penido M**, **Alon US**. Phosphate homeostasis and its role in bone health. *Pediatr Nephrol*. 2012;27(11):2039–2048.
56. **Maré AD**, **D'Haese PC**, **Verhulst A**. The role of sclerostin in bone and ectopic calcification. *Int J Mol Sci*. 2020;21(9):E3199.
57. **Beck-Nielsen SS**, **Mughal Z**, **Haffner D**, **et al**. FGF23 and its role in X-linked hypophosphatemia-related morbidity. *Orphanet J Rare Dis*. 2019;14(1):58.
58. **Xin W**, **Yuan S**, **Wang B**, **Qian Q**, **Chen Y**. Hsa_circ_0066523 promotes the proliferation and osteogenic differentiation of bone mesenchymal stem cells by repressing PTEN. *Bone Joint Res*. 2021;10(8):526–535.
59. **Zhao D-W**, **Ren B**, **Wang H-W**, **et al**. 3D-printed titanium implant combined with interleukin 4 regulates ordered macrophage polarization to promote bone regeneration and angiogenesis. *Bone Joint Res*. 2021;10(7):411–424.
60. **Chen X**, **Chen W**, **Aung ZM**, **Han W**, **Zhang Y**, **Chai G**. LY3023414 inhibits both osteogenesis and osteoclastogenesis through the PI3K/Akt/GSK3 signalling pathway. *Bone Joint Res*. 2021;10(4):237–249.
61. **He Z**, **Nie P**, **Lu J**, **et al**. Less mechanical loading attenuates osteoarthritis by reducing cartilage degeneration, subchondral bone remodelling, secondary inflammation, and activation of NLRP3 inflammasome. *Bone Joint Res*. 2020;9(10):731–741.
62. **Brzeszczyńska J**, **Brzeszczyński F**, **Hamilton DF**, **McGregor R**, **Simpson A**. Role of microRNA in muscle regeneration and diseases related to muscle dysfunction in atrophy, cachexia, osteoporosis, and osteoarthritis. *Bone Joint Res*. 2020;9(11):798–807.
63. **Yu H**, **Zhang J**, **Liu X**, **Li Y**. microRNA-136-5p from bone marrow mesenchymal stem cell-derived exosomes facilitates fracture healing by targeting LRP4 to activate the Wnt/β-catenin pathway. *Bone Joint Res*. 2021;10(12):744–758.
64. **Cheng B**, **Wen Y**, **Yang X**, **et al**. Gut microbiota is associated with bone mineral density: an observational and genome-wide environmental interaction analysis in the UK Biobank cohort. *Bone Joint Res*. 2021;10(11):734–741.
65. **Li J**, **Ho WTP**, **Liu C**, **et al**. The role of gut microbiota in bone homeostasis. *Bone Joint Res*. 2021;10(1):51–59.
66. **Li S**, **Mao Y**, **Zhou F**, **Yang H**, **Shi Q**, **Meng B**. Gut microbiome and osteoporosis: a review. *Bone Joint Res*. 2020;9(8):524–530.



**Author information:**
- M. C. M. Li, BEng, MSc, PhD Candidate
- S. K-H. Chow, BSc, MSc, PhD, Research Assistant Professor
- R. M. Y. Wong, MBChB, PhD, Assistant Professor (Clinical)
- J. C. Y. Cheng, MD, MBBS, Emeritus Professor
- L. Qin, BA, MPhil, PhD, Professor
- W-H. Cheung, BSc, PhD, Professor

  Musculoskeletal Research Laboratory, Department of Orthopaedics and Traumatology, The Chinese University of Hong Kong, Hong Kong, China.
- B. Chen, MD, PhD, Professor, Department of Spine Surgery, The First Affiliated Hospital of Sun Yat-sen University, Guangzhou, China.


**Author contributions:**
- M. C. M. Li: Conceptualization, Data curation, Formal analysis, Methodology, Investigation, Project administration, Writing – original draft.
- S. K-H. Chow: Conceptualization, Methodology, Project administration, Resources, Writing – review & editing.
- R. M. Y. Wong: Writing – review & editing.
- B. Chen: Writing – review & editing.
- J. C. Y. Cheng: Conceptualization.
- L. Qin: Funding acquisition.
- W-H. Cheung: Conceptualization, Funding acquisition, Project administration, Resources, Supervision, Writing – review & editing.


**Funding statement:**
- The authors disclose receipt of the following financial or material support for the research, authorship, and/or publication of this article: funding support from General Research Fund (Ref: 14113018) and Areas of Excellence Scheme (AoE/M-402/20).


**Data sharing:**
- The protocol was prepared before the study. Study data are available from the corresponding author upon reasonable request.


**Acknowledgements:**
- The authors would like to acknowledge Prof. K. S. Leung, Prof J. C. Y. Cheng, and Miss. V. M. H. Choy for their contributions.


**Ethical review statement:**
- This study was carried out following research ethics guidelines by the Animal Experimentation Ethics Committee of The Chinese University of Hong Kong.


**Open access funding**
- The authors report that they received open access funding for their manuscript from The Chinese University of Hong Kong (General Research Fund, Ref: 14113018).